scientific reports

Check for updates

OPEN

Preclinical pharmacology characterization of HX009, a novel PD1 x CD47 Bi-specific antibody

Hang Ke[1], Tao Yang[1], Faming Zhang[1], Cen Chen[1], Jingjing Wang[2], Jinping Liu[2], Xiaoyu An[2], Lingxin Xiong[2], Xianfei He[3], Lei Zhang[1] & Qi-Xiang Li[1]✉

Certain immune-checkpoint inhibitors have a narrow therapeutic window (TW) as cancer therapeutics, and engineered dual-/multi-targeting agents could potentially widen the TW to bring true clinical benefits. We report a new rationally-designed bispecific-antibody (BsAb), HX009, simultaneously targeting PD1 and CD47 to improve both the efficacy and safety over the respective single-targeting agents by grafting the extracellular domain of SIRPα onto the parental anti-PD1-monoclonal antibody, HX008. This resulted in an IgG4-based "2 × 2" symmetric structure but with an intentionally-reduced CD47-binding affinity, suggesting a novel candidate cancer immunotherapy. Specifically, HX009 has binding affinity constant of 8.951×10^{-9} M for human PD1 and 2.557×10^{-8} M for human CD47, respectively, where the CD47 binding is significantly weaker as compared to the binding affinity of HX008 to PD1 as well as the binding affinity of SIRPα-Fc to CD47, leading to little binding to RBCs and platelets and is contrasting to many CD47-agents in development. However, HX009 effectively and simultaneously binds to the PD1 and CD47 on $PD1^{+}CD47^{+}$ T-cells via *cis*-binding and elicits enhanced T cell activation compared to the parental HX008. HX009 caused little cytokine-release in human peripheral blood mononuclear cells. HX009 cross-species binds to cynomolgus monkey PD1/CD47 but not to rodents, making cynomolgus monkeys the choice of species to investigate the pharmacokinetics (PK) and toxicology of HX009. HX009's anti-tumor activities were confirmed in several humanized preclinical mouse models by determining either its anti-PD1 (humanized hu-CD47-MC38 models) or anti-CD47 (HuT-102 lymphoma CDX and three PDX-AML models) functions, although limited available humanized models have hindered broadly demonstration of enhanced anti-tumor activities contributed from the dual targeting of the BsAb. The expanded DLBCL-PDX trial data suggested that both EBV-status and OX40 expression could potentially be two positive predictors for response to HX009. An intravenous (IV) infusion PK study in cynomolgus monkey revealed its largely vasculature distribution, terminal half-life ($T_{1/2}$) of ~ 50 h, and dose-proportional exposure without accumulation. The anti-drug antibody (ADA) was observed in all monkeys as expected, affecting the PK parameters of repeated administration. The IV single-dose toxicology study with a 14-day observation revealed a maximum tolerated dose of 150 mg/kg, while the repeated-dose (once weekly for 4 weeks, 5 doses in total) study showed a highest non-severely toxic dose (HNSTD) of 15 mg/kg. The desired preclinical PK and safety profiles, along with its antitumor activity, support HX009's candidacy for its clinical development.

Keywords Innate/adaptive ICIs, BsAb, Xenograft and humanized syngeneic tumor models, Immunotherapy, Toxicology, Pharmacokinetics, Anti-tumor activity, AML, Cynomolgus monkey

CD47, a "don't eat me" receptor broadly/over-expressed in many human tumors[1–7], has recently been recognized not only as a key innate, but also adaptive, immune checkpoint[8–10]. High expression of CD47 has also frequently been associated with poor prognosis of various types of cancers. CD47 and its ligand, signal regulatory protein α (SIRPα) which resides on the surface of phagocytic cells (macrophages/DCs), are considered promising cancer immunotherapy targets[1,9,11]. However, many CD47-targeting agents (monoclonal antibody (mAb) or fusion proteins) have met significant challenges in clinical development without a single approval due to marginal anti-tumor activity as a single agent[12,13] and significant dose-limiting toxicity (DLT), mostly hematotoxicity such as anemia and/or thrombocytopenia[13]. Several strategies have been considered to overcome these challenges,

[1]Hanx Pharmaceuticals, Inc, Hangzhou, China. [2]Crown Bioscience, Inc, Taicang, China. [3]Shanghai Model Organisms Center (SMOC), Shanghai, China. ✉email: henry.li@hanxbio.com

including masked binding epitopes, multi-targeting (functions), tumor-specific targeting, and reduced binding affinity to red blood cells (RBCs) and megakaryocytes. In clinical practice, CD47-agents have also frequently been attempted to combine with other modalities to increase efficacy[3,14,15].

PD1/PD-L1 is one of the most important adaptive immune-checkpoints, whose blockers have enjoyed great success in the clinic and have been approved for the treatment of a broad range of malignancies. These immune-checkpoint inhibitors (ICIs) restores anti-tumor immunity by reversing the exhaustion of effector T cells (T_{eff}) within tumor microenvironment (TME). However, the majority of treated patients responded poorly[16]. Interestingly, a recent report described that insufficient expression of SIRPα in melanoma cells might have attributed to the poor response to PD-1 inhibitors in many melanoma patients[10]. This observation led to the theory that simultaneous targeting of PD1 and CD47 on the T_{eff} in TME would be responsible for the long-term reversal of exhaustion of T_{eff}, which was confirmed in a preclinical setting by the dual-targeting of $CD8^+$ T_{eff} via PD1 monoclonal antibody (mAb) and the genetic overexpression of SIRPα on the surface of melanoma cells[10].

The combination of PD1/PD-L1 blockers with other anticancer modalities, including other ICIs of different mechanisms of actions (MOAs), e.g. CTLA4 and CD47, etc., can potentially increase clinical benefits and expand indications. Considering that CD47/SIRPα is an innate immune-checkpoint, it is reasonable to hypothesize that the combination of PD1/PD-L1 blockers and CD47/SIRPα blockers could productively increase the clinical applications/benefits. However, we need to realize that a simple combination, although it might benefit anti-tumor efficacy, may usually not improve safety over the respective single-agent treatments. Considering the above-mentioned PD1-/CD47-dual targeting of T_{eff} for long-term reversal of T_{eff}-cell exhaustion[10], we can further hypothesize that PD1 × CD47 dual-targeting bispecific antibody (BsAb) could have greater immunotherapeutic effect over PD1-mAbs, so a potentially "enhanced PD1 molecule". On the other hand, the BsAb can also be engineered such to minimize the hematological toxicity of the CD47-targeting.

We previously reported a novel BsAb dual-targeting CD47 and PD1, HX009, with enhanced anti-lymphoma activities among a collection of different preclinical lymphoma models, suggesting that it may be a potential new anti-lymphoma treatment if confirmed in clinic[17]. However, this early report has yet to reveal much of the detailed molecular parameters of HX009 as per design, along with its contributions to the enhanced safety profiles in the preclinical settings, both in vitro and in vivo, as well as its potentially new MOAs. The earlier report has yet to demonstrate a robust predictive biomarker for the response of lymphoma to HX009, which can be explored to develop companion diagnostic for guiding future clinical trial. The present report attempted to detail the rational design of HX009, to create a safer and more effective biological candidate for the treatment of cancers beyond lymphoma and also provide practical guidance to guide clinical development.

Results

Generation of HX009, a BsAb dual-targeting PD1 and CD47

Previously we mentioned that we created a new BsAb targeting both PD1 and CD47, HX009[10], by grafting the extracellular CD47-binding domain of SIRPα to the C-terminus of the HX008 (Pucotenlimab) heavy chain with minor modifications in the Fc-region[18–21] to generate a "2 × 2" symmetric molecular structure, as shown in Fig. 1A. In the HX009 design, IgG4 was chosen to diminish Fc-mediated antibody-dependent cellular cytotoxicity (ADCC) and complement-dependent cellular cytotoxicity (CDC) in order to avoid a T_{eff} depleting function due to the presence of PD-1 on T_{eff} cells[21,22]. The original high PD1 binding affinity of HX008 was maintained, not only as an effective blocker for PD1 and PD-L1 interaction but also with tumor-targeting properties because upregulated PD1 expression is usually present on the exhausted T cells within the tumor microenvironment (TME), instead of circulating T cells in the peripheral. On the other hand, CD47 binding affinity was significantly reduced compared to native SIRPα or $SIRP_{\alpha}$-Fc, thus minimizing the hematologic toxicity that is commonly seen in the first generation of anti-CD47 agents[13,23]. We hypothesized that such designed BsAb could still have high avidity ("apparent affinity") to bind to the T_{eff} cells because of the *cis*-binding of PD-1 and CD47, where high-binding affinity to PD1would be the driver binder of the BsAb. HX009 BsAb protein was readily produced from a recombinant CHO-K1 cell line stably expressing the BsAb construct. The final HX009 fusion protein was identified and characterized by size exclusion chromatography (SEC-HPLC) and capillary electrophoresis sodium dodecyl sulfate (CE-SDS) with adequate stability and purity (Supplement Table S1 and Supplement Figure S1A-C), both heavy chain and light chain amino acid sequence was identified (Supplement Table S2) and its deglycosylated molecular weight (MW) was determined to be 173,162.34 Daltons by LC–MS (Supplement Figure S1D).

Confirmation of the designed receptor binding affinity

Next, we systematically evaluated the potential of HX009 as a pharmaceutical candidate. The binding affinity of an antibody to its target protein is one of the key pharmacological properties determining its efficacy and toxicity. In our previous reported work, we have investigated HX009 target affinity using enzyme-linked immunosorbent assay (ELISA) as measured by EC_{50} and fluorescence-activated cell sorting (FACS) method for cell surface binding[17]. In order to precisely understand the detailed intrinsic binding properties to the ligand protein, we performed biochemical binding characterization of HX009 to determine its target receptor-binding affinity constant as measured by K_D using surface plasmon resonance (SPR) assay. Our results showed that the K_D for human PD1-his recombinant protein is around 8.951×10^{-9} M and the K_D for human CD47 recombinant protein is around 2.557×10^{-8} M, respectively (Table 1). This data confirmed our intended design, which is to maintain a similar and strong affinity for PD1 as the parental PD1 HX008 mAb but to significantly reduce the affinity for CD47, which is largely consistent with the results of ELISA-based binding assays described before[17]. The relatively lower affinity for CD47 versus high affinity for PD1 also makes PD1 the primary targeting driver for HX009, so as to target tumor microenvironment (TME) where PD1 is upregulated.

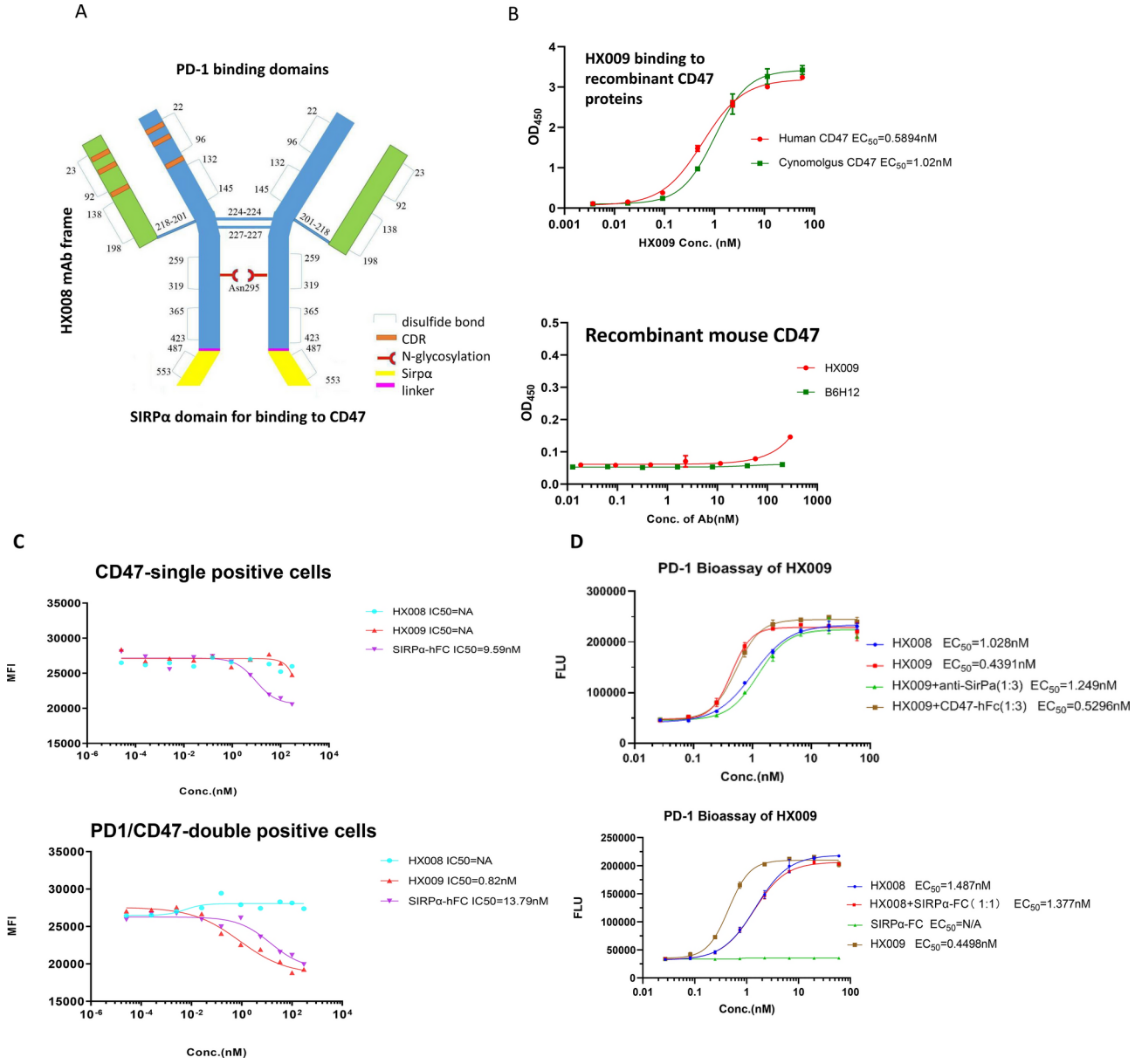

Fig. 1. HX009 structure and in vitro characterization. (**A**) Molecular structure of HX009: 2×2 symmetric BsAb molecule; (**B**) HX009 binding to the recombinant CD47 proteins of different species including human, cynomolgus monkey (upper) and mouse (lower), binding EC_{50} (half maximal effective concentration) were determined per four-parameter equation fitting curves; (**C**) competitive binding to CD47 single-positive (upper panel) or CD47-PD1 double positive (lower panel) cells by HX009. Labeled B6H12 (anti-CD47) was competed out by SIRPα-Fc, but not by HX009 (weakened binding) in single-positive cell assay, while it was competed out in double-positive cell assays by both SIPRα-Fc and HX009. (**D**) T-cell activation luciferase report assays: upper panel: HX009 had enhanced T-cell activation (*cis*-binding) over HX008 (4X), whereas the enhancement is diminished by an anti-SIRPα neutralizing antibody but not by CD47-Fc (soluble CD47). Lower panel: there was no enhancement of T-cell activation by HX008 and SIRPα-Fc combo treatment due to *trans*-binding.

We also assessed HX009 cross-species binding affinity constants to both PD1 and CD47 recombinant proteins from non-human primate (NHP) and rodents, in order to select relevant animal models to support HX009 in vivo pharmacology evaluation. The SPR results are shown in Table 1 and Supplement Figure S2, where HX009 showed a reduced binding affinity to cynomolgus monkey PD1 and CD47 as compared to the human counterparts (PD1: 3.865×10^{-7} M vs. 8.951×10^{-9} M; CD47: 1.338×10^{-7} M vs. 2.557×10^{-8} M), but HX009 hardly binds to rat and mouse PD1 and CD47. In addition, we also investigated cross-species binding affinity with the receptors of cynomolgus monkeys and rodents using ELISA, a previously described method[17]. Our data demonstrated that HX009 does bind to CD47 recombinant proteins from cynomolgus monkey, where the affinity is slightly weakened (EC_{50} ~ 1.02 nM for cynomolgus monkey vs. EC_{50} ~ 0.59 nM for human) (Fig. 1B

Receptors	SPR platform	Ka (1/Ms)	Kd (1/s)	KD (M)
huCD47	Biacore	4.82×10^{5}	1.23×10^{-2}	2.56×10^{-8}
huPD-1	Biacore	1.33×10^{5}	1.19×10^{-3}	8.95×10^{-9}
cynoCD47	Biacore	8.91×10^{4}	1.19×10^{-2}	1.34×10^{-7}
cynoPD-1	Biacore	2.32×10^{4}	8.96×10^{-3}	3.87×10^{-7}
muPD-1	Biacore	N/A	N/A	N/A
muCD47	Biacore	N/A	N/A	N/A
raPD-1	Biacore	N/A	N/A	N/A
raCD47	Biacore	N/A	N/A	N/A
huC1q	ProteOn	N/A	N/A	N/A
huCD16a	ProteOn	N/A	N/A	N/A

Table 1. Determination of affinity constant of HX009 binding to its target receptors. *hu* human, *cyno* cynomolgus monkey, *mu* mouse, *ra* rat.

upper panel). We then tested the HX009 affinity to mouse CD47 together with another high affinity anti-human CD47 monoclonal antibody, B6H12. Neither HX009 nor B6H12 bound to mouse CD47 (Fig. 1B lower panel). Altogether, these data show that HX009 has a slightly reduced binding affinity constant (KD) to cynomolgus monkey CD47 than that of humans, but no cross-species binding to rodent CD47. Therefore, cynomolgus monkeys could be relevant species for preclinical pharmacokinetics (PK), toxicology, and immunogenicity evaluations of HX009 to support future clinical testing.

HX009 binds efficiently to the surface CD47 on the PD1/CD47 double-positive cells than the single-positive cells
We have previously demonstrated that HX009 binds to each receptor in single-positive cells (Raji-B $CD47^{+}$ or Jurkat $PD1^{+}$) and double-positive cells (HEK293T-PD1 cell line)[17]. Next, we performed a competitive cell binding assay to investigate HX009 binding efficiency (avidity). We fluorescently labeled B6H12 mAb, which could bind to either CD47 + single or CD47 + PD1 + double positive cells even in the presence of the competing HX009 due to its high CD47 binding affinity. We found that in the single positive cell binding assay, the binding of B6H12 mAb to $CD47^{+}$ single positive cells cannot be affected by HX008 PD1 mAb due to the absence of PD1 in the cells, but could be readily eliminated by SIRPα-Fc fusion protein (Fig. 1C upper panel). This is in contrast to that HX009 cannot efficiently compete out B6H12 due to the significantly lower binding affinity (weakened) to CD47, as compared to SIRPα-Fc. However, in the $CD47^{+}PD1^{+}$ double positive cell binding assay, the binding of B6H12 mAb to CD47/PD1 double-positive cells can be competed out by both SIRPα-Fc fusion protein and HX009 (Fig. 1C lower panel), suggesting that the apparent binding affinity or avidity of HX009 to CD47/PD-1 double-positive cells is significantly enhanced by the *cis*-binding of HX009 to both PD-1 and CD47 molecules on the cell surface driven by high affinity to PD-1.

HX009 elicits stronger T-cell activation signals in the double-positive reporter cell than parental HX008
Previously, we observed HX009 mediated T-cell activation in a double-positive reporter cell, confirming the PD1 targeting mediated T-cell activation[17]. However, to our surprise, we consistently observed higher T-cell activation (2.5–3 times lower EC_{50} value) for HX009 than for HX008[17]. This prompted us to hypothesize that the additional activation beyond that of HX008 resulted from the efficient *cis*-binding of HX009 to CD47 in the T-cell-derived reporter cell line. To test this hypothesis, we added a competing anti-SIRPα mAb in the assay, which efficiently neutralized the CD47 targeting function of HX009, resulting in activation levels similar to those of HX008 (Fig. 1D upper panel). This suggested that enhanced T-cell activation resulted from the binding of HX009 to both PD1 and CD47 simultaneously on the reporter cell surface. On the other hand, adding a soluble-CD47 protein in the assay, instead of the anti-SIRPα mAb, cannot competitively block T cell activation by HX009, suggesting that CD47 on T-cells has significantly higher avidity binding to HX009 than that of soluble CD47 (Fig. 1D lower panel). This is because the binding of CD47 on the T cell surface to HX009 is efficient *cis*-binding, whereas the binding of soluble CD47 to HX009 is not. Moreover, when we tested the combination treatment of HX008 and SIRPα-Fc fusion protein, although SIRPα-Fc had 10 times higher affinity for CD47 than HX009, the combination treatment did not show enhanced activation over HX008 single treatment, suggesting that the anti-PD1 and anti-CD47 combination treatments did not yield the same effect as our PD-1 × SIRPα BsAb (Fig. 1D lower panel). This supports the hypothesis that efficient *cis*-binding of HX009 to CD47 on the T-cell surface is required for enhanced T-cell activation, which is consistent with the hypothesis proposed by others[10].

In vitro assays for the potential toxicity of HX009

One of the major challenges for first-generation of CD47-targeting agents is their dose-limiting toxicity (DLT) resulting from systemic binding to non-tumor tissues, mainly hematotoxicity, e.g. anemia and thrombocytopenia due to the high CD47 expression in RBCs and megakaryocytes. Our rationally designed HX009 with reduced CD47 binding affinity, described above and elsewhere[17], should have minimized RBC/platelet binding. In vitro RBC and platelet binding assays were performed to assess the binding of HX009 to human RBCs and platelets, along with a control magrolimab, an investigational anti-CD47-IgG4 type antibody in the clinics[3,14] which is known to bind to RBCs/platelets. The results confirmed that the binding of HX009 to RBCs was minimal

(Fig. 2A) and that the binding of HX009 to platelets (Fig. 2B) was drastically reduced compared to that of magrolimab. Next, we incubated cells with PNGase-F, an effective enzyme for N-linked oligosaccharide removal, and found that HX009 binding to RBC did not seem to increase, suggesting that the minimized RBC binding was not due to excessive glycosylation blockade from the CD47 surface (Fig. 2A). Altogether, HX009 is unlikely to cause anemia and thrombocytopenia when administered at a defined dose, in contrast to magrolimab. In other words, HX009 may not induce DLT in clinics in effective dose ranges. Furthermore, HX009 was constructed on an IgG4 frame containing an inert Fc to minimize ADCC/CDC effects which is thought to be a potential source of hematoxicity. HX009 demonstrated little binding to the gamma Fc receptor (Fcγ) RIIIA (CD16a, FcγRIIIA), a key Fc receptor for ADCC activity, with the binding kinetics curves shown in Fig. 2C. CD16a and C1q binding affinity constants were determined by SPR and the results showed that there was no apparent binding (Table 1 and Supplement Figure S2). Our data suggest that HX009 should have minimized ADCC/CDC in humans, similar to the parental molecule HX008.

Immunotoxicity, e.g. induction of cytokine release syndrome (CRS), also called cytokine storm, by a large biologic, can be assessed in vitro using solid- and liquid-phase methods, as well as using phytohemagglutinin (PHA) or Staphylococcal enterotoxin B (SEB) treatment as positive controls. The CRS assay results showed that the expression levels of IL2, IL4, IL10, TNFα, IFNγ, and IL17A from two donors' PBMCs upon the HX009 treatment were in the range of 0–1.64 pg/mL, both by solid-phase and liquid-phase methods. In contrast, IL2, IL4, IL6, IL10, TNFα, and IFNγ levels were significantly higher in the SEB treatment group (Fig. 2D). In the blood samples from normal subjects, the reference ranges for these seven cytokines were 6.970–10.829 pg/mL for IL-2, 4.752–6.504 pg/mL for IL-4, 5.760–12.906 pg/mL for IL-6, 4.332–7.216 pg/mL for IL-10, 5.723–12.878 pg/mL for TNF-α, 2.950–4.697 pg/mL for IFN-γ, and 7.945–10.910 pg/mL for IL-17A, respectively. In our experiment, the mean values of IL-2, IL-4, IL-6, IL-10, TNF-α, IFN-γ, and IL-17A secretion were within the normal range, suggesting that HX009 is unlikely to cause a cytokine storm when tested in humans.

HX009 demonstrated strong anti-tumor activities in preclinical tumor models of both solid tumors and hematological malignances

Next, we tested the antitumor activity of HX009 in preclinical cancer models. Since the syngeneic colon cancer model MC38 is known to be sensitive to PD1-mAb treatment[17], we first employed a humanized MC38-huCD47

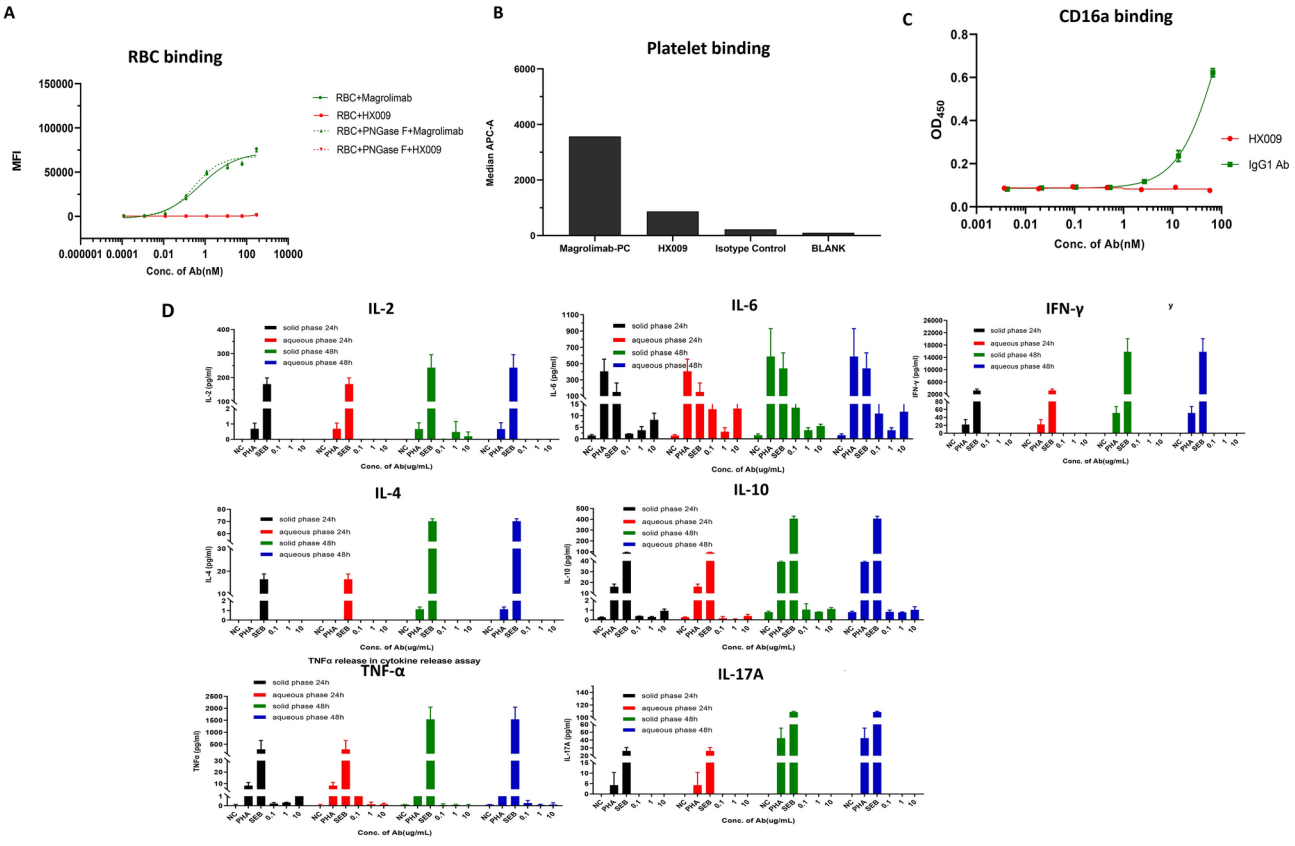

Fig. 2. In vitro toxicity assays of HX009. (**A**) HX009 binding to RBC in vitro as measured by flow cytometry, with or without PNGase-F pretreatment, with Magrolimab positive being experimental control, MFI: mean fluorescence intensity; (**B**) HX009 binding to platelets as assayed by flow cytometry; (**C**) Binding to FcγRIIIa (CD16a) via ELISA method, where a human IgG1 antibody was used as positive control; (**D**) In vitro cytokine release from PBMC induced by HX009 with solid phase or liquid phase. Cytokines including IL-2, IL-4, IL-6, IL-10, IL-17α, TNF-α and IFN-γ were investigated by CBA flow cytometry.

model to test anti-solid tumor activity of HX009. In this model, MC38 tumor cells stably overexpressing human CD47 were inoculated into human PD-1 HuGEMM mice, in which the extracellular domain of mouse PD-1 was replaced with a human counterpart[26]. The results demonstrated that anti-PD1 mAb (Keytruda) treatment caused an anticipated antitumor response in this model (Fig. 3A), and HX009 also caused similar antitumor activity. In contrast, SIRPα-Fc seemed to have little anti-tumor activity in this solid tumor model, and the combination treatment of SIRPα-Fc and Keytruda did not cause a greater anti-tumor response than Keytruda alone, as expected. In other words, this model may only be able to evaluate the antitumor activity contributed by anti-PD1 functions, but not from anti-CD47. One interpretation is that mouse SIRPα cannot cross-react with human CD47 on MC38 cells, and the other is that anti-CD47 alone is insufficient to cause anti-tumor activity in the MC38 model.

To ensure that the above observations are reliable, we employed a new model with more comprehensive humanization: the same MC38-huCD47 tumor cells were inoculated in human PD-1/PD-L1/SIRPα/CD47 quadruple knock-in HuGEMM mice. Our results demonstrated that HX009 induced slightly higher antitumor activity than HX008, although the difference was modest and not statistically significant (Fig. 3B). This more complete humanization may be more suitable for the pharmacological evaluation of HX009 BsAb. Altogether, our data confirmed that the antitumor activity of HX009 observed in these two in vivo models is attributed to its anti-PD1 function.

Since many investigational anti-CD47 agents are being tested in clinics for the treatment of hematopoietic malignancies, including lymphoma and acute myeloid leukemia (AML)[4,6,15,23–25], we assessed the potential definitive contribution of the anti-CD47 function of HX009 to its anti-tumor activity in models of hematological malignances, which may be more sensitive to anti-CD47 targeting. Since polymorphic SIRPα in NOD mice interacts with human CD47[26,27], the anti-CD47 function, but not the anti-PD-1 function of HX009, could be evaluated in blood cancer xenografts in NOD/SCID immunodeficient mice. Our previous report[17] has investigated the anti-tumor effects of HX009 in many lymphoma xenograft models in NOD/SCID mice. In the present study, we tested the anti-leukemic activity of HX009 in three patient-derived AML xenografts (PDX) that we previously described[28]. These three AML-PDXs had different levels of CD47 protein in the following order: AM7577 > AM5512 > AM8096 (Fig. 3C). In these systemic models, leukemic loads were represented by the percentage of human CD45 positive cells in peripheral blood, as shown in Fig. 3C. Two intraperitoneal administrations of HX009 at 10 mg/kg significantly delayed tumor growth in all three AML-PDX models (Fig. 3C, left column). In addition, HX009 treatment seemed to prolong animal survival (Fig. 3C middle column). These results confirm the anti-leukemic role of HX009 via its anti-CD47 function. Moreover, the relative anti-leukemic activity of HX009 seemed to correlate with CD47 protein levels in these three models (Fig. 3C, bottom table), suggesting that CD47 could potentially serve as a predictive biomarker for HX009 in clinical trials. In addition, at the termination, organs of the animals, including the bone marrow (BM), spleen (SP), liver, or peripheral blood (PB), etc., were harvested to determine the leukemia loads in these organs. Notably, while the leukemic loads were reduced significantly in peripheral organs (SP or PB), the leukemic loads in the bone marrow showed little change in response to HX009 treatment, similar to Ara-C chemotherapy (Supplement Figure S3A), but different from other targeted agents, e.g. AC220[28]. One of the possibilities is that antibody drugs may not penetrate the bone marrow efficiently. Together with the MC38-huCD47 and HuT-102 in vivo results (Supplement Figure S3B), we can conclude that HX009 has antitumor activity attributed to both its anti-PD1 and anti-CD47 functions. This is also consistent with our previously reported work on the anti-lymphoma activities of HX009 in a selection of lymphoma CDX and PDX models[17] and confirmed the designed anti-tumor activity of HX009.

OX40-expressions seem to be good positive predictors for DLBCL-PDX responses to HX009

Our previous report described HX009 anti-lymphoma pharmacology trial on a small collection of seven DLBCL-PDXs and demonstrated the anti-lymphoma activities of HX009 in some of them, due to the anti-CD47 function of HX009 (no contribution from anti-PD1 because of the lack of T-cells in these xenograft models)[17]. Although we hinted a possible role of CD47-expression in predicting tumor responses[17], we did not have sufficient data to conclude the claim. In the present investigation, we expanded the trial cohort to 23 DLBCL-PDXs plus three xenograft lymphomas (Fig. 3D). The TGI results as shown in Supplement Figure S2A still did not show statistical significance between TGI and CD47 mRNA expression (Supplement Figure S4A). Furthermore, we have also performed the same analysis on the other target gene expression (PD-L1), and the results demonstrated no statistical significance between TGI and PD-L1 mRNA expression (Supplement Figure S4B).

On the other hand, recent report by others suggested a possible correlation between ICI efficacy and expression of OX40 in mRNA/protein in DLBCL-patients[29], which promoted us to examine our HX009-DLBCL-PDX trial data. The results seemed to confirm that tumor responses were correlated to the OX40 expression with statistical significance in our mouse trial (Fig. 3D). In addition, the OX40-mRNA levels in 58 DLBCL-PDX cohort, inclusive of those 23 PDXs in trial, seem also to correlate with the PD-L1-mRNA levels (Supplement Figure S4C), which is consistent with other reports that OX40-expression correlates with that of other immune ICIs, positively predicting the response to ICI in patients[29]. It worth pointing out the tested two PTCL xenograft models Karpas-299 (ALCL)[17] and HuT-102 (a HTLV-Tax expressing T-cells, and shown in Fig. 3D), also express high levels of OX40, in consistent with the results of DLBCL-PDX trial. Altogether with the consideration of CD47-targeting in these models and PD1-targeting in patients, OX40-expressing lymphoma patients would likely be more responsive to HX009 than those without OX40-expression.

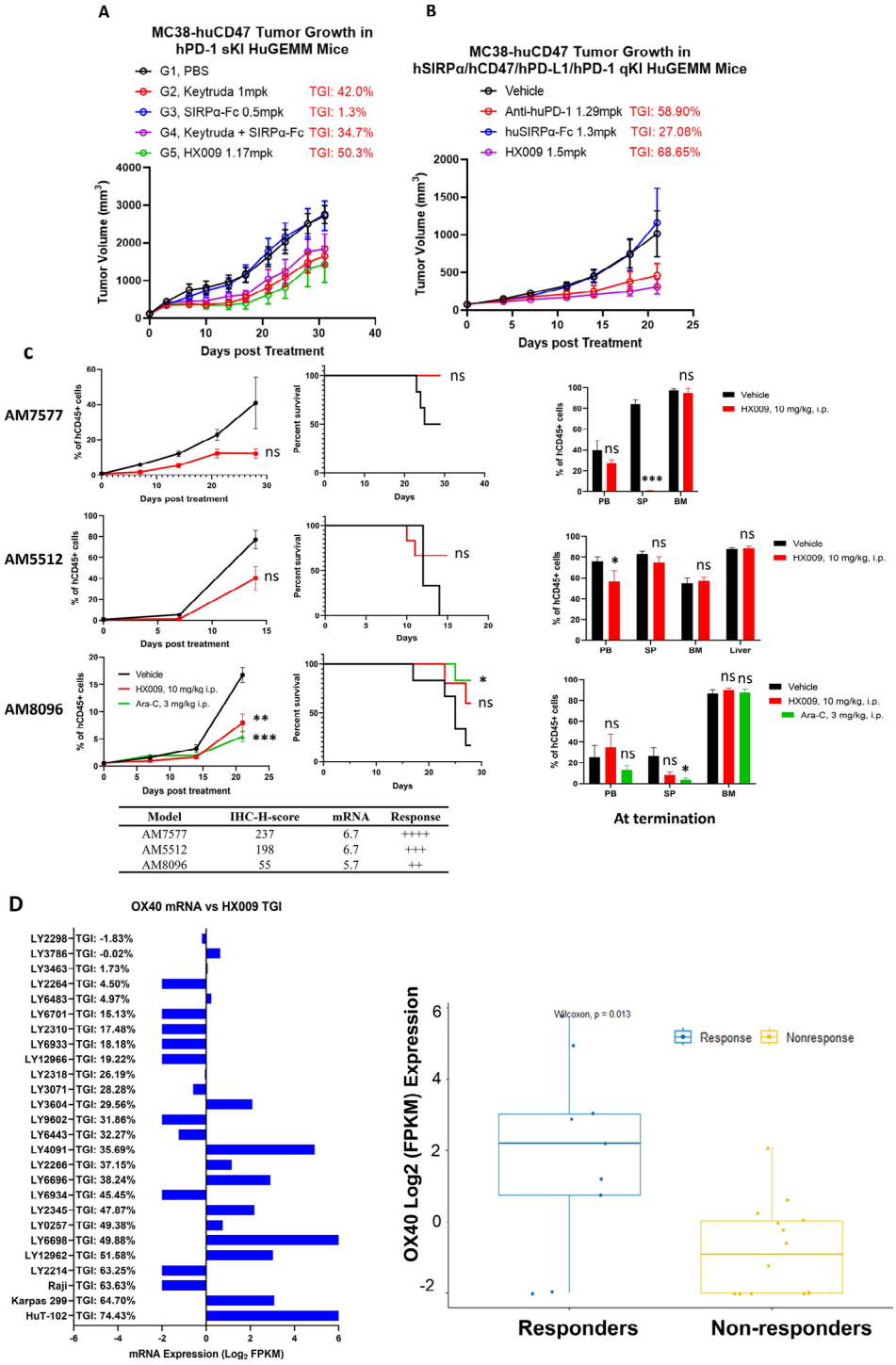

Fig. 3. HX009 anti-tumor pharmacology studies in preclinical cancer models. (**A**) Pharmacology evaluation of HX009 in a humanized MC38-huCD47 mouse colon cancer model in huPD1-HuGEMM mice; (**B**) Pharmacology evaluation of HX009 in a humanized MC38-huCD47 mouse colon cancer model in huPD1 × huPD-L1 × huCD47 × huSIRPα-HuGEMM model; (**C**) Pharmacology evaluation of HX009 in three AML-PDX models as shown in the figures. Columns from Left to right: Leukemic burden was measured as percentage of human $CD45^+$ cells in peripheral blood; survival was displayed as in Caplan-Meier plot; Leukemic loads in different organs at the termination, as % of human $CD45^+$. *SP* spleen, *BM* bone marrow, *PB* peripheral blood. Bottom: The differential expressions of CD47 per IHC and RNAseq in three AML-PDX models are shown in the bottom table. Graphs in A-D showed mean tumor volume ± standard error of the mean (SEM). Significance was calculated using one-way ANOVA with post-hoc comparisons or Welch's *t*-test between treatment groups and vehicle group. ns, no significance; $^*p < 0.05$; $^{**}p < 0.01$; $^{***}p < 0.001$. (**D**) Correlation of OX40 mRNA levels with HX009 anti-lymphoma activity represented by TGI (tumor growth inhibition) in DLBCL-PDX trial.

HX009 demonstrates adequate pharmacokinetic (PK) profile in cynomolgus monkey model as a candidate biologic

One of the important features of antibody drug based on nature molecule (*e.g.* mAb) is its preferred PK profile (e.g. long and consistent half-life). However, BsAb like HX009 as an artificially engineered product, although constituting of combined natural molecules, may not necessarily maintain such preferred PK profiles. Preclinical understanding of the PK profile of a BsAb candidate can help to determine whether or how it can be developed into an investigational drug for clinical testing. Cynomolgus monkeys were chosen for the preclinical PK evaluation of HX009 for the following reasons: (1) reasonably similar binding affinities for both PD1 and CD47 receptors between cynomolgus monkeys and humans, as shown in Fig. 1B and Table 1; (2) the high homology between human and cynomolgus monkeys in PD1 and CD47 sequences (Supplement Figure S5); and (3) cynomolgus monkeys being the most commonly used species in monoclonal antibody studies with a large amount of historical data for reference. An ELISA-based bioanalytical method for detecting and quantifying the concentration of HX009 in monkey serum was developed and validated. We performed two PK studies of HX009 based on our intended clinical testing plan: a single IV infusion study and a repeated IV infusion study, as outlined in Supplement Table S3.

HX009 concentrations in blood at different time points were determined by ELISA, as shown in Fig. 4. The key PK parameters of single dose of HX009 in cynomolgus monkeys are summarized in Table 2 and Figs. 4A–C. Specifically, the mean terminal elimination half-life ($t_{1/2}$) from the three single dosing groups were 50.74, 55.49 and 53.37 h, respectively. The mean residence time (MRT_{last}) was 60.21, 61.08 and 63.06 h, respectively. The mean clearance (CL) were 1.09, 0.98 and 0.77 mL/h/kg, respectively, indicating a slow elimination of HX009 from the body. The mean steady-state volume of distribution (Vss) was 75.19, 74.85 and 59.63 mL/kg, respectively, indicating that the HX009 injection was mainly distributed in the blood. The mean area under curve until last time point ($AUC_{0\text{-}last}$) were 907.85, 2867.98, and 12,396.69 h*μg/mL, respectively. The mean total area under curve ($AUC_{0\text{-}\infty}$) were 967.12, 3103.89, and 13,285.42 h*μg/mL, respectively. Mean maximum serum concentration (C_{max}) values were 17.34, 52.98, and 222.41 μg/mL, respectively. The $AUC_{0\text{-}last}$ ratio was 1:3.16:13.65, the $AUC_{0\text{-}\infty}$ ratio was 1:3.21:13.74, and the C_{max} ratio was 1:3.06:12.83, suggesting dose-dependent exposure to HX009 in cynomolgus monkeys (Figs. 4A–C). There seemed to be little difference in the PK parameters between the two sexes for the three dose levels in general. Linear analysis of LnDose and $LnAUC_{last}$ using WinNonlin software showed linear kinetics in cynomolgus monkeys within a dose range of 1–10 mg/kg. In summary, the preferred PK profile of HX009 BsAb in the preclinical setting is reasonably maintained, consistent with general antibody drug PK profile.

For multiple dose study, after the first dose, the mean terminal elimination half-life ($t_{1/2}$) was 57.49 h, the mean residence time (MRT_{last}) was 49.49 h, the mean clearance (CL) was 1.30 ml/h/kg, the mean apparent volume of distribution at steady state (V_{ss}) was 93.43 ml/kg, the mean C_{max} was 44.41 μg/ml, and the mean

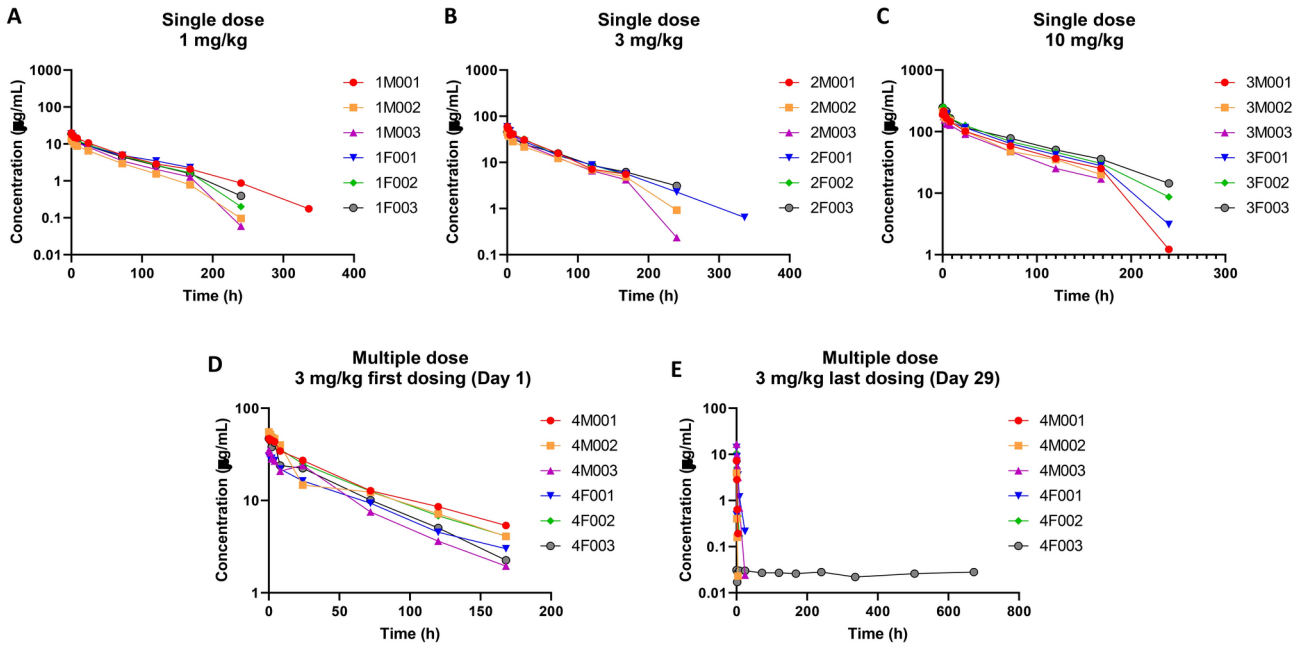

Fig. 4. Individual blood drug concentration–time curve after single intravenous injection of HX009 in cynomolgus monkeys. (**A**) Intravenous (IV)-PK dose regimens. (**B**–**D**) The serum concentration–time curves of HX009 in individual animal following a single IV infusion at 1 mg/kg, or 3 mg/kg, or 10 mg/kg. (**E**) The serum concentration–time curves of HX009 in individual animal after the first dose in the repeated dose PK study. (**F**) The serum concentration–time curves of HX009 in individual animal after the last dose in the repeated dose PK study. Reference animal numbers are listed in the figures, e.g. 1M001 indicates the first male monkey in the first group, 1F001 indicates the first female monkey in the first group.

Group/dose level	Sex	$t_{1/2}$ (h)	T_{max} (h)	C_{max} (μg/mL)	AUC_{last} (h*μg/mL)	$AUC_{0-\infty}$ (h*μg/mL)	CL (mL/h/kg)	Vss (mL/kg)	MRT_{last} (h)
Group 1 (1 mg/kg)	M	41.82 ± 10.02	0.389 ± 0.529	16.21 ± 3.19	861.71 ± 275.33	868.90 ± 280.22	1.23 ± 0.37	74.83 ± 11.43	60.86 ± 10.41
	F	59.67 ± 25.32	0.083 ± 0.000	18.47 ± 0.32	953.99 ± 28.77	1065.34 ± 142.58	0.95 ± 0.12	75.55 ± 15.94	59.56 ± 1.75
	M + F	50.74 ± 19.80	0.236 ± 0.374	17.34 ± 2.37	907.85 ± 182.23	967.12 ± 226.09	1.09 ± 0.29	75.19 ± 12.41	60.21 ± 6.71
Group 2 (3 mg/kg)	M	45.82 ± 9.03	0.722 ± 1.107	51.09 ± 7.39	2658.96 ± 235.07	2827.27 ± 449.66	1.08 ± 0.16	72.68 ± 10.25	57.14 ± 7.32
	F	65.16 ± 10.22	0.083 ± 0.000	54.88 ± 7.91	3077.01 ± 159.41	3380.50 ± 96.70	0.89 ± 0.03	77.02 ± 9.48	65.03 ± 12.70
	M + F	55.49 ± 13.66	0.403 ± 0.782	52.98 ± 7.16	2867.98 ± 291.03	3103.89 ± 420.04	0.98 ± 0.15	74.85 ± 9.15	61.08 ± 10.23
Group 3 (10 mg/kg)	M	48.90 ± 8.66	0.389 ± 0.529	210.53 ± 6.96	10,390.66 ± 1448.57	11,372.19 ± 911.30	0.88 ± 0.07	64.99 ± 9.26	56.22 ± 7.49
	F	57.83 ± 12.37	0.389 ± 0.529	234.30 ± 27.08	14,402.73 ± 1164.57	15,198.66 ± 1788.47	0.66 ± 0.08	54.28 ± 2.96	69.90 ± 4.14
	M + F	53.37 ± 10.73	0.389 ± 0.473	222.41 ± 21.96	12,396.69 ± 2492.15	13,285.42 ± 2450.34	0.77 ± 0.14	59.63 ± 8.50	63.06 ± 9.24
Group 4 (3 mg/kg) (Day 1)	M	62.13 ± 13.84	0.083 ± 0.000	45.76 ± 10.18	2184.65 ± 448.73	2547.12 ± 675.89	1.24 ± 0.34	92.09 ± 3.68	49.71 ± 5.38
	F	52.85 ± 8.03	0.083 ± 0.000	43.06 ± 11.40	2037.37 ± 418.04	2282.25 ± 490.07	1.35 ± 0.27	94.78 ± 23.59	49.26 ± 2.53
	M + F	57.49 ± 11.32	0.083 ± 0.000	44.41 ± 9.78	2111.01 ± 396.17	2414.68 ± 547.58	1.30 ± 0.28	93.43 ± 15.17	49.49 ± 3.77
Group 4 (3 mg/kg) (Day 29)	M	1.44 ± 1.22	0.083 ± 0.000	9.30 ± 6.59	18.07 ± 22.02	18.07 ± 22.02	498.47 ± 503.99	324.85 ± 128.27	1.33 ± 1.35
	F	1639.39 ± 2834.20	2.722 ± 4.571	8.23 ± 7.32	24.19 ± 24.10	94.64 ± 106.42	83.43 ± 84.66	33,332.42 ± 57,252.06	113.47 ± 191.77
	M + F	820.41 ± 2004.48	1.403 ± 3.232	8.77 ± 6.26	21.13 ± 20.92	56.35 ± 80.51	290.95 ± 395.16	16,828.64 ± 40,471.91	57.40 ± 135.96

Table 2. Mean PK parameters after a single and multiple IV injection of HX009 injection at each dose level in cynomolgus monkeys (Mean ± SD). For Group 4, the AUC_{last} term should be AUC_{0-168}.

AUC_{0-168} was 2111.01 h*μg/ml (Table 2). The PK parameters of individual animals after the last dose were quite different, mainly due to the production of anti-drug antibodies (ADA) by animals. There was no gender difference in the PK parameters either after the first or last dose ($p > 0.05$). After multiple administrations, the accumulation factor was in the range of 0.00–0.03, indicating that drug exposure after the last dose was lower than that after the first dose (Figs. 4D, E). In other words, there was no drug accumulation in the animals.

Immunogenicity study in monkeys have also been conducted by measuring the production of anti-drug antibody (ADA). Notably, all animals produced ADA (Supplement Table S4), which can potentially be explained by species differences in the immune system between humans and monkeys, since HX009 is a humanized antibody/human fusion proteins which would be less immunogenic in human[30] as compared to in monkey here. After multiple IV injections of 3 mg/kg drugs, the kinetic characteristics HX009 were affected by ADA production, resulting in large individual differences in kinetic parameters. The significant PK variations in this repeated dose preclinical study may not reflect those in the human studies due to the anticipated less ADA production in human[30].

HX009 demonstrated preferable toxicology profile in cynomolgus monkey model as a candidate biologic

Since the toxicity profiles of anti-CD47 antibodies or SIRPα fusion proteins, mainly hematotoxicity, are generally known to be undesirable/intolerable[13], as compared to those of PD1 antibodies, one of the main designed features of HX009 BsAb is to minimize the hematotoxicity, which need to be first confirmed in animal models in the preclinical setting before it can be tested as an investigational drug candidate in the clinics. We thus set out to perform toxicology assessment of HX009, aiming at revealing the nature, degree, dose–effect and time-effect relationship, reversibility of potential toxic effects, and target organs/tissues of toxicity. The relationship between exposure and toxic effects was also assessed via toxicokinetic investigation. Similarly, cynomolgus monkeys have been used in toxicology studies under GLP compliance. Two toxicological studies were designed as follows (Supplement Table S5): (1) a single IV dose study of 75 and 150 mg/kg, followed by 14 consecutive days of monitoring; and (2) a multiple IV dose study of 3, 15, or 50 mg/kg for four consecutive weeks (a total of five doses).

After a single IV administration of HX009, there had been no mortality or significant toxicity observed at the highest dose (150 mg/kg). The maximum tolerated dose (MTD) is determined to be 150 mg/kg. On Day 15 of the study, gross examination revealed no abnormal changes in the size, shape, color, and texture of major organs and tissues (e.g., heart, liver, spleen, lungs, kidneys, pancreas, gastrointestinal tract, reproductive system, and injection site). Histopathological examination revealed several changes at the administration site (Supplementary Table S6). One monkey (1/3) in the HX009 75 mg/kg group had mild subcutaneous mononuclear cell infiltration at the administration site, and one monkey (1/3) in the HX009 150 mg/kg group had mild subcutaneous inflammation and mild subcutaneous mononuclear cell infiltration at the administration site. It is not certain whether the above changes resulted from mechanical irritation or HX009.

For the repeated-dose toxicity study, in the 50 mg/kg group, death/moribundity was observed in three monkeys (one possibly related to nephrotoxicity, and the other two seems to "infusion-like" respiratory depression) after 3rd dose and 4th dose, respectively, likely due to the production of ADA. In the 15 mg/kg and middle 50 mg/kg dose groups, mild decreases in erythroid series (RBC, HGB, and HCT) and PLT were observed by hematology tests, and mild mononuclear cell infiltration in the brain (meninges) was observed by histopathological examination during the dosing periods, but not during the recovery period. The observed minor hematoxicity of anemia and/or thrombocytopenia for HX009, assumed to be resulted from SIRPα's effect,

are in contrast to other known anti-CD47 agents, e.g. magrolimab and TTI-621[31], etc. There were no significant abnormal changes in the general physical conditions of the animals, including body weight, food intake, body temperature, ophthalmic examination, ECG, respiratory rate, urinalysis, immune complexes, lymphocytes/monocytes, bone marrow smear examination, organ weight, and coefficient. The highest non-severely toxic dose (HNSTD) was determined to be 15 mg/kg. The majority of monkeys in the 3, 15, and 50 mg/kg groups developed anti-drug antibodies at the final administration time point (Supplementary Table S4), which was consistent with the PK study. Increased receptor occupancy of HX009 was observed in all monkeys administered with HX009 injection during the dosing and recovery phases (Supplement Table S7). For monkeys in control and HX009 injection groups, cytokines parameters of TNF-α, IFN-γ, IL-2, and IL-10 were below the lower limit of quantification or without apparent abnormalities during the dosing and recovery phases. An increase trend was noted in IL-6 for all the monkeys within 2 h after the 5th dosing with HX009 injection, but rapidly return to normal level. There was no abnormality in IL-6 at the end of recovery phase (Supplement Table S8). All above cytokine data indicates low risk triggering CRS in the repeated-dose toxicity study. ADA was found in most of the monkeys treated with HX009 injection on Day 14 and almost all the monkeys treated on Day 21–84 (Supplement Table S9).

Toxicokinetics (TK) of HX009 cynomolgus monkeys

In addition to the general PK assessment of HX009, it is also important to understand its toxic exposure of HX009. To this end, blood samples from the repeat-dosing toxicology studies were collected to determine the drug exposure PK parameters, as shown in Table 3. After the first dose, the mean C_{max} and AUC_{last} of the different dose groups are shown in Table 3, with dose-proportionality and likely little gender difference. The mean C_{max} and AUC_{last} values after the last dose are shown in Table 3. These exposure values were correlated with toxicity and mortality to understand the toxic exposure of HX009. After five weeks of continuous administration in cynomolgus monkeys, the exposures (C_{max} and AUC_{last}) (Table 3) were significantly lower than those observed after the first dose, suggesting that there was no significant accumulation and that the lowered exposures may be related to the fact that ADA accelerated drug clearance.

A safety pharmacology study was also performed concurrently with repeat IV dose toxicology studies at doses of 3, 15, and 50 mg/kg. Under these dose conditions (once weekly for four consecutive weeks), HX009 had no significant effect on blood pressure, respiratory rate, or other ECG parameters for each monkey group. Overall, our PK and toxicology studies demonstrated adequate PK and well-tolerated toxicology profiles of HX009, supporting further human trials, thus validating our early hypothesis that this rationally designed BsAb is indeed safe in preclinical studies.

Discussion

First-generation CD47-targeting agents, including CD47 mAbs[3,15] and SIRPα-fusion proteins[32,33], many of which are IgG1 based, encounter major safety challenges. Most such agents have yet to demonstrate sufficient clinical benefits due to narrow therapeutic windows (TW) as a single agent treatment of either hematological malignancies or solid tumors in clinics[3,14]. Combination treatments, particularly with other ICIs, may enhance efficacy[8,9,34,35] but may not improve safety. On the other hand, BsAbs of CD47, together with other targeting agents, may improve both safety and efficacy profiles, and many of such bispecific molecules are currently under investigation in the clinics[8,23,35]. We hypothesized that a bi-functional molecule dual-targeting PD1 × CD47 by rational design could potentially improve both the efficacy and safety profile over the first-generation agents. We thus constructed HX009 BsAb to achieve this objective according to the following rationales: (1) HX009 BsAb improves safety since PD1-antibody can target to TME where it is highly expressed, contrasting to little expression in peripheral blood, as seen in other BsAb[36]; (2) we chose PD1 and CD47 blockade for fulfilling dual targeting innate/adaptive immune checkpoints[8,9]; (3) we chose PD1 over PD-L1[8,34] for avoiding "antigen-sink" effect often associated with PD-L1 antibodies due to broad expression among normal tissues and the need to target both PD-L1 and -L2; (4) IgG4, instead of IgG1, was chosen to reduce the hematoxicity caused by CD47 targeting; (5) SIRPα is fused to the C-terminus of heavy chain (Fc) so to reduce CD47 binding, thus the binding to RBCs/platelets, as similarly by others[35,36]; (6) efficient *cis*-binding to CD47 in T-cells[10]. This report performed comprehensive pharmacology assessment of HX009 both in vitro and in vivo. Our results, together with another separate report[17], largely confirmed our working hypothesis that PD1 × SIRPa BsAb has: (a) minimized binding to RBCs and platelets in vitro and hematological toxicity in vivo, and (b) increased anti-tumor effect attributed to the dual-targeting in the preclinical modeling. This rationally designed molecule behaved as desired.

First-generation CD47 targeting agents, exemplified by CD47 monoclonal antibodies, are broadly being tested in clinics, mostly for hematopoietic malignancies, e.g. AML and lymphoma. Most such trials require combination treatments to yield meaningful clinical benefits, if any[3,14,33]. In addition, most of the combinations caused even severe toxicity. Therefore, thus far none of these agents has obtained regulatory approval. HX009 itself, being a dual targeting agent, is more likely to yield meaningful clinical benefits as a "monotherapy". Our early report[17] demonstrated enhanced and robust anti-lymphoma activity, seemingly contributed from both targeting MOAs[17]. This report also further expanded indication into solid tumor and AML models at preclinical settings. Thus, HX009 warrants further clinical development as an investigational drug for the treatment of different malignancies, either in the form of a single agent treatment or in combination with other therapies, including ADC. Currently, HX009 is undergoing extensive clinical study in patients with different types of NHLs and solid tumors (ClinicalTrials.gov Identifier: NCT05189093).

In particular, the anti-lymphoma activities seemed to be correlated with the levels of OX40 in the lymphoma, which may enable patient selection via companion diagnostics, thus accelerating robust clinical development. OX40, a type I transmembrane glycoprotein also known as CD134 or tumor necrosis factor receptor superfamily member 4 (TNFRSF4), is an immune co-stimulatory receptor, together with its ligand OX40L, forming OX40-

Dose level	Sex	Day1				Day29				AR		
		T_{max} (h)	C_{max} (μg/mL)	AUC_{last} (h*μg/mL)	N	T_{max} (h)	C_{max} (μg/mL)	AUC_{last} (h*μg/mL)	N	C_{max}	AUC_{last}	N
3 mg/kg	M	1.213 ± 1.631	56.22 ± 4.83	3214.10 ± 360.51	5	0.033 ± 0.000	14.15 ± 7.76	34.90 ± 22.76	3	0.24 ± 0.11	0.01 ± 0.01	3
	F	0.420 ± 0.530	51.65 ± 10.98	2771.49 ± 745.73	5	0.033 ± 0.000	15.31 ± 3.84	46.99 ± 23.92	3	0.35 ± 0.16	0.02 ± 0.02	3
	F + M	0.817 ± 1.217	53.93 ± 8.35	2992.80 ± 599.45	10	0.033 ± 0.000	14.73 ± 5.51	40.95 ± 21.91	6	0.30 ± 0.14	0.02 ± 0.01	6
15 mg/kg	M	0.613 ± 0.530	348.96 ± 38.48	20,537.81 ± 1715.63	5	0.033 ± 0.000	43.54 ± 35.21	151.76 ± 173.91	5	0.13 ± 0.12	0.01 ± 0.01	5
	F	0.613 ± 0.530	380.01 ± 50.62	23,489.82 ± 5234.36	5	0.033 ± 0.000	117.20 ± 108.21	1219.94 ± 2072.25	5	0.32 ± 0.30	0.05 ± 0.08	5
	F + M	0.613 ± 0.499	364.48 ± 45.44	22,013.81 ± 3988.22	10	0.033 ± 0.000	80.37 ± 85.22	685.85 ± 1496.31	10	0.23 ± 0.23	0.03 ± 0.06	10
50 mg/kg	M	0.420 ± 0.530	1167.70 ± 95.57	87,209.34 ± 4415.53	5	0.275 ± 0.484	913.39 ± 564.62	27,996.20 ± 37,411.91	4	0.75 ± 0.45	0.32 ± 0.43	4
	F	0.420 ± 0.530	1234.16 ± 134.14	84,926.08 ± 8105.55	5	0.355 ± 0.558	1076.35 ± 542.42	18,800.29 ± 14,903.19	3	0.85 ± 0.41	0.22 ± 0.19	3
	F + M	0.420 ± 0.499	1200.93 ± 115.25	86,067.71 ± 6270.04	10	0.309 ± 0.472	983.23 ± 514.84	24,055.10 ± 28,249.28	7	0.80 ± 0.40	0.27 ± 0.33	7

Table 3. Mean TK parameters and accumulation ratio of HX009 injection groups after the first and last dosing (Mean ± SD). AR indicates the accumulation ratio, which indicates the C_{max} ratio and AUClast ratio compared between the last and first dosing; N: indicates the number of animals.

OX40L trimer–trimer complex between the surface of T-cells (OX40) and APCs/NKs (OX40L). OX40 only expressed on the surface of activated $CD4^+/CD8^+$ T cells, and expresses constitutively on T_{reg} as well as on conventional T_{eff}, particularly within TME. OX40/OX40L interactions directly triggers conventional T cell activation via NF-*k*B1 pathway and inhibits bcl-x and survivin to prevent apoptosis; and it also downregulates FoxP3/CTLA4, thus T_{reg} function[37,38]. It worth noting that OX40 as a T-cell activation marker has not particularly appreciated as a marker on B-lineage of lymphoma, and this line of research could have important implication in the future treatment of B-lymphoma. An OX40-IHC and OX40-RT-qPCR assay could also be adopted as another companion diagnostics in the clinics.

Our safety data presented in this report, either in vitro or in NHP in vivo indeed confirmed that the reduced CD47 binding affinity could be a viable approach to reduce systemic hematologic toxicity of CD47 targeting as indeed verified in our phase I trial[30]. If HX009 eventually demonstrated superior anti-tumor activities in patients, it could be potentially the first group of anti-CD47 agents that can practically benefit cancer patients.

Our preliminary observations of enhanced T-cell activation in the in vitro T-cell activation assay seemed to confirm the importance of PD1 × CD47 dual-targeting in re-activation of T-cells as reported by others[10]. This could be an important novel MOA of HX009 that could potentially benefit the treatment in the clinic if proven, certainly warranting further investigations.

Materials and methods

Cells and animals

CHO-K1 cells were purchased from ATCC (American Type Culture Collection) and acclimated in-house for producing antibody proteins. CHO-PDL1-CD3L cells and Jurkat-PD1-NFAT cells were provided by China National Institutes for Food and Drug Control (NIFDC). 293 T, Jurkat and Raji cells were provided by China Center for Type Culture Collection (CCTCC). huPD-1 HuGEMM mice were provided by Jiangsu Biocytogen Co. Ltd. Human PD-1/PD-L1/SIRPα/CD47 quadruple knock-in HuGEMM mice were provided by human PD-1/PD-L1/SIRPα/CD47 quadruple knock-in HuGEMM mice. Cynomolgus monkeys were purchased from Hainan Primate Laboratory Animal Development Co., Ltd., and pharmacokinetics study and GLP toxicology studies were conducted in West China-Frontier PharmaTech Co., Ltd. (National Chengdu Center for Safety Evaluation of Drugs).

Size exclusion high performance liquid chromatography (SEC-HPLC)

HX009 was diluted to 5.0 mg/mL with mobile phase buffer (25 mM of phosphate, 0.3 M NaCl, pH6.8). 10μL of samples were loaded onto buffer pre-equilibrated chromatographic column (TSKgelG3000SWXL, Tosoh, 7.8 × 300 mm, 5 μm). Samples were flowed at rate 0.7 ml/min at room temperature and analyzed in HPLC (1260Bio, Agilent). High-molecular weight (HMW area) species and monomer (Main peak area) purities were calculated respectively by area normalization method.

Capillary electrophoresis with sodium dodecyl sulfate (CE-SDS)

For non-reduced CE-SDS, the sample preparations were performed using SDS-MW kit (Beckman). 200 μg of protein samples were mixed with SDS-MW buffer and 0.04 M of iodoacetamide and incubated at 65 °C for 5 min. Supernatant were taken after 10,000 rpm centrifuge. The sample were then loaded onto capillary electrophoresis (PA800plus, Beckman Coulter) at 20 °C for 35 min under 15 kV voltage. The monomer (Main peak area) was calculated in nrCE-SDS by area normalization method. For reduced CE-SDS (rCE-SDS), the sample preparation was performed using SDS-MW kit (Beckman). 200 μg of protein samples were mixed with SDS-MW buffer and 5% of β-mercaptoethanol and incubated at 17 °C for 15 min. Supernatant were taken after 10,000 rpm centrifuge. The samples were then loaded onto capillary electrophoresis (PA800plus, Beckman Coulter) at 20 °C for 30 min under 15 kV voltage. The monomer (Main peak area) was calculated in nrCE-SDS by area normalization method. The total percentage of heavy chain and light chain signal (HC + LC) was regarded as HX009 purity. The non-glycosylated heavy chain (NGHC) percentage was also reported.

Deglycosylated molecular weight measurement

The de-glycosylated complete molecular weight of HX009 was analyzed by electrospray ionization four-pole time-of-flight mass spectrometry (6530B ESI-Q/TOF, Agilent). 250ug of HX009 was diluted with buffer (1 M ammonium bicarbonate solution 2.5ul, glycosidase 2.5ul (enzyme: sample = 1:100)) to make the final concentration of 5 mg/ml. Samples were then incubated in water bath for 3 h at 37 °C, and then samples were diluted to 1 mg/mL for analysis.

Determination of the affinity constant of HX009 binding to different receptor proteins

The affinity constants were determined using SPR method via two platforms: Biacore T200 (GE) and ProteOn XPR36 (Bio-rad). Biacore T200 platform was used to determine the binding affinity of HX009 to PD-1 and CD47 receptors in different species. By coupling the 7.5 μg/mL of HX009 antibody on the chip surface, the recombinant human (Atagenix), cynomolgus monkey (Acrobiosystems), mouse (Sinobiological) and rat (Sinobiological) CD47 proteins, at serial loading concentrations from 2 to 128 nM (two-fold dilution), or the recombinant human (Atagenix), cynomolgus monkey (Sinobiological), mouse (Sinobiological) and rat (Sinobiological) PD1 proteins at serial loading concentrations from 1 to 64 nM (two-fold dilution), flowed through the chip surface, a binding of 200-s to reach the target level above 770 RU, and a 20-min dissociation time with 10 mM of Glycine pH 1.7. Data acquisition and analysis were performed using Biacore T200 Control Software. To determine the affinity constants of human CD16a and C1q, SPR analysis was assessed using ProteOn XPR36. HX009 at 25 nM was immobilized on the chip surface using a standard amino coupling method to saturate its binding to the chip surface. The antibody was bound to the human CD16a (Acrobiosystems) at a series of 53.625–858 nM (two-

fold dilution) or human C1q (Fitzgerald) at a series of 6.25–100 nM (two-fold dilution) at an flow rate 30 μL/min, binding time of 200 s, and sufficient dissociation time. Data acquisition and analysis were performed using ProteOn Manager software.

Target protein binding assay based on ELISA

Human (Atagenix), cynomolgus monkey (Acrobiosystems), mouse (Sinobiological) CD47, and human CD16a (Sinobiological) recombinant proteins were coated onto 96-well plates at 4 °C overnight. Serial dilutions of HX009 or other control proteins were added to duplicate wells and incubated for 1 h. The bound antibodies were detected using horseradish peroxidase (HRP)-conjugated goat anti-human or anti-mouse antibodies (Jackson ImmunoResearch) and developed using 3,3′5,5′-tetramethylbenzidine (TIMB, Biosharp) substrates. The binding EC_{50} (half maximal effective concentration) of HX009 to the human target antigen was determined by fitting the dose–response data to a four-parameter stimulation model.

Antibody binding avidity assay

Human CD47-single expressing 293 T cells or PD1/CD47-double expressing 293 T-PD1 cells were incubated with various concentrations of the reference samples (HX008 and SIRPα-Fc) and HX009 (~ 300–0.00003 nM) at 4 °C for 1 h. The cells were then incubated with 15 nM mouse anti-human CD47 antibody B6H12 at 4 °C for 1 h. Bound antibodies were detected with Alexa Fluor® 647-conjugated AffiniPure Goat Anti-Mouse IgG (H + L) secondary antibody (Jackson Immuno Research) and analyzed by flow cytometry. IC_{50} values were calculated from the best-fit binding curves using GraphPad Prism software.

PD-1 luciferase reporter potency assay

CHO-PDL1-CD3L cells engineered to express human PD-L1 and TCR were plated in 96-well polystyrene microplates and incubated at 37 °C in 5% CO_2 for 18 h. On day 2, cell culture media were removed and Jurkat-PD1-NFAT cells, engineered to carry human PD1 and an IL-2 promoter-guided luciferase reporter gene, were added to the wells to mix with CHO-PDL1-CD3L cells. Test samples of different concentrations (approximately 60–0.027 nM) were then added and incubated at 37 °C in 5% CO_2 for a 6 h. For competition tests, anti-SIRPα or CD47-hFc (competing agent vs. test sample concentration: 1:3) was added to the reaction to compete with HX009. For the combination treatment, an equal concentration (1:1) of SIRPα-hFc was added to the reaction mixture and co-incubated with HX008. The luciferase readout was detected by measuring chemiluminescence at a 560 nM wave length using a Bio-LiteTM Luciferase Assay System (Vazyme, Nanjing). The dose–response curve was fitted using a four-parameter simulation equation. EC_{50} values were calculated from the best-fit binding curves using GraphPad Prism software.

RBC/platelet binding assay

RBC were isolated from healthy donor blood, leukocytes and monocytes were removed using Ficoll density gradient separation (GE), and RBC remained at the bottom layer of gradient separation. RBC were pre-incubated with or without 1000 U/mL PNGase F for 24 h. The RBC were then incubated with different concentrations of HX009 at 4 °C for 60 min. Cell binding was detected using APC-labeled anti-human Fc flow cytometry. Platelets were isolated from healthy donors using ficoll density gradient separation (GE) to remove red blood cells RBC and leukocytes and were incubated with 200 nM of HX009 at 4 °C for 60 min. Cell binding was detected using APC-labeled anti-human Fc flow cytometry. Platelets were gated as $CD45^{-}CD41^{+}$.

In vitro cytokine release assay of human immune cells

Human PBMC were isolated from healthy donors using Ficoll density gradient separation (GE) and incubated with different concentrations of HX009 via the solid phase or liquid phase method. For the HX009 solid-phase method (HX009 is immobilized to the membrane), HX009 diluted in a gradient of 10, 1, 0.1 μg/mL with PBS buffer was added onto 96-well plates for coating to the well surface. After coating at 4 °C overnight, the upper liquid was discarded and replaced with the freshly prepared PBMC suspension. For the liquid phase method (HX009 is in solution), PBMC were incubated with freshly prepared HX009 at final concentrations of 10, 1, 0.1 μg/ml. PBMC were also treated with PHA (10 μg/mL), SEB (100 ng/mL), or media in both solid- and liquid-phase samples, together with the corresponding positive controls and negative controls. Released cytokines were detected in the supernatant after 24 h and 48 h of incubation at 37 °C. A cytometric bead array (CBA) assay kit (BD Pharmingen) was used for cytokine detection via flow cytometry, following the manufacturer's instructions. After samples were collected (FCS2.0 format), standard curve drawing and data analysis were performed using CBA special analysis software FCAP Array v1.0. Value 0 means the data was below lower limit of quantification.

Pharmacokinetic study

Twenty-four adult cynomolgus monkeys were randomly divided into four groups per body weight/sex: 1, 3, and 10 mg/kg for single intravenous (IV) administration, and 3 mg/kg repeated IV dosing (weekly, five times), with six monkeys/group, half males and half females. HX009 was dosed at 5 mL/kg, and dosing lasted ~ 30 min for each monkey. Blood was collected from the saphenous vein of the lower limb, and serum was prepared by immediate centrifugation, followed by freezing at −80 °C. The time points to collect blood samples for single administration were pre-dosing and 5 min, 1, 2, 4, and 8 h, and 1, 3, 5, 7, 14, and 28 days post-dosing. The time points to collect blood samples for repeated administration were pre-first dosing and 5 min; 1, 2, 4, 8 h; 1, 3, 5, and 7 days post-first dosing; pre-third dosing; pre-fourth dosing; pre-fifth dosing and 5 min; 1, 2, 4, and 8 h; and 1, 3, 5, 7, 14, and 28 days post-fifth dosing. The concentration of HX009 in monkey serum was determined using ELISA. The relevant pharmacokinetic parameters were calculated using WinNonlin (Pharsight) 6.4; anti-drug

antibodies in cynomolgus monkey serum samples were detected and measured by bridging-ELISA. The study was performed in a facility under Good Laboratory Practice (GLP).

The concentration of HX009 in monkey serum was determined using ELISA. Human CD47 protein (1 μg/mL) was coated onto a microtiter plate as a capture reagent. After blocking, the standard curve samples, quality control samples, and samples to be tested were added to the microtiter plate for incubation, allowing HX009 to bind to the capture antigen to form an antigen–antibody complex and thus immobilize on a 96-well plate. After washing to remove the unbound HX009 injection, PD1-his antigen was added to allow binding to two antigenic determinants. The secondary antibody HRP-66005 (Proteintech) was added to allow binding to the antigen–antibody complex captured on the microtiter plate, followed by an additional stop solution to terminate the color development reaction. The optical density (OD) value at 450 nm was measured, and the concentration of HX009 was positively correlated with the color intensity produced by the final reaction.

Anti-drug antibodies (ADA) in cynomolgus monkey serum samples were detected by bridging-ELISA. HX009 was coated onto a microplate. Then, HX009 bound to ADA from monkey serum prepared in the PK studies and was incubated with biotinylated-HX009 to form a complex of "Drug–ADA–Drug–Biotin." Streptavidin-HRP was added to amplify the detection signal, and TMB was added for chromogenic reaction, followed by an additional stop solution to terminate the color development reaction. The optical density value was measured at a wavelength of 450 nm. The OD values were positively correlated with ADA concentrations in the positive quality controls or study samples.

Toxicological and toxicokinetics study

Six adult cynomolgus monkeys were randomly divided into two groups for a single administration of low-dose (75 mg/kg) or high-dose (150 mg/kg) HX009. Each group contains to females and one male monkey. Animals were sacrificed 15 days after dosing for anatomical examination. During the study, body weight, food uptake, respiratory frequency, and blood pressure were examined regularly, and ECG data were evaluated. All surviving animals were sampled for hematology and clinical chemistry analyses on days 2 and 14. Urinalysis was performed on all the surviving animals on day 13.

For repeated administration toxicological studies, 40 adult cynomolgus monkeys were randomly divided into four groups: control (excipient solution without drug), low-dose (3 mg/kg), moderate-dose (15 mg/kg), and high-dose (50 mg/kg) HX009 administration; each group contained five female and five male monkeys. Animals were sacrificed after an 8-weeks recovery phase for anatomical observation. Injection was dosed at 5 mL/kg, and dosing lasted ~ 30 min for each monkey. During the study, body weight, food uptake, respiratory frequency, and blood pressure were checked regularly, and ECG data were evaluated. All surviving animals were sampled for hematology analysis on days 3 and 7, 1 days after the 3rd and 5th dosing, and 1 day before the recovery phase necropsy. All surviving animals were sampled for clinical chemistry analysis 1 d after the 3rd and 5th dosing, and 1 day before the recovery phase necropsy. Urinalysis for all surviving monkeys was conducted on Day 28 and before the recovery phase of the necropsy. All surviving animals were sampled for the determination of ADA in serum before the first dosing, on days 14, 21, and 28, and on recovery days 28 and 55. All surviving animals were sampled for lymphocyte subset flow cytometry prior to the 1st dosing (the 2nd sampling in the acclimation phase), 1 day after the 3rd and 5th dosing, and then 1 day before the recovery phase necropsy. All surviving monkeys were sampled for cytokine analysis via the MSD method at predose and about 1, 2, 8, and 24 h postdose of the 1st and 5th dosing, at approximately 24 h after the 3rd dosing, and at 1 d before the recovery phase necropsy. All surviving animals were sampled for the determination of receptor occupancy at pre-dose, 1.5–2.5 and 24 h post-dose of the 1st dosing, on days 7, 14, 28, and recovery days 14 and 55. Ocular examination was conducted on all surviving animals within three days before the dosing and recovery phase necropsies. Bone marrow smears for all animals to be sacrificed were prepared on the day of scheduled necropsies. For toxicokinetic studies, blood samples were collected from all surviving animals administered HX009 injection at predose and 0 min, 1 h, 4 h, 24 h, 72 h, and 168 h post-dose of the 1st and 5th dosing. For control animals, blood was sampled pre-dose and 0 min post-dose of the 1st and 5th dosing. The HX009 serum concentration was detected by ELISA with manipulation similar to that described in the PK studies. The study was performed in a facility under Good Laboratory Practice (GLP) and was also reported in accordance with the ARRIVE guidelines.

In vivo mouse anti-tumor pharmacology modelling

All procedures of in vivo pharmacology were performed under sterile conditions at the Crown Bioscience and Biocytogen SPF facility and conducted in strict accordance with the Guide for the Care and Use of Laboratory Animals of the National Institutes of Health. The protocol was approved by the Committee on the Ethics of Animal Experiments of Crown Bioscience (Crown Bioscience IACUC Committee) and Biocytogen. The humane management and euthanasia of experimental animals in the following in vivo animal models complied with the provisions of the Animal Welfare Act (9CFR) and the regulations of the American Veterinary Association on euthanasia (AVMA 2020). Briefly, mice reached humane endpoints were euthanized by overdose carbon dioxide. In addition, a second euthanasia operation (e.g., cervical dislocation) was used to ensure that the animal dies. Anticancer pharmacology studies in mouse models were conducted by essentially following standard pharmacology protocols that have been widely described[28,39,40] with certain modifications and were also reported in accordance with the ARRIVE guidelines.

Specifically, a humanized syngeneic mouse MC38-huCD47[39,41] model was constructed by knock-in (KI) the huCD47 gene into a mouse syngeneic MC38 CRC cell line, and human PD1 was knocked-in C57BL/6 mice (huPD-1 HuGEMM mice), similar to those used by others[42]. MC38-huCD47 tumor cells were subcutaneously injected into the right flank of huPD-1 HuGEMM mice for tumor development. Once the tumor sizes reached approximately 120 mm^3, 40 tumor-bearing mice were enrolled and randomized into five groups (N = 8 per

group) according to their tumor size and body weight. Following randomization, mice in each group received their designated treatments as follows: vehicle, IP (intraperitoneal), twice weekly; Keytruda, 1 mg/kg, IP, twice per weekly; hSIRPα-Fc, 0.5 mg/kg, IP, twice per weekly; HX009, 1.17 mg/kg, IP, twice weekly. Tumor volumes and body weights were measured twice per week, and tumor growth inhibition (TGI) was used to determine the anti-tumor activities of each test reagent. The TGI was calculated as $TGI\% = (1 - V_{treatment}/V_{control}) \times 100\%$. This hCD47-MC38 humanized syngeneic model was constructed at Biocytogen.

Similarly, MC38-huCD47 tumor cells were inoculated into the right flank region of huPD-1/huPD-L1/huSIRPα/huCD47quadraple knock-in HuGEMM mice for tumor development. Once the tumor sizes reached approximately 80 mm^3, 24 tumor-bearing mice were enrolled and randomized into four groups (N = 6 per group) according to their tumor size and body weight. Following randomization, the mice in each group received their designated treatments as follows: vehicle, IP, twice weekly; HX008 (anti-huPD-1 mAb), 1.29 mg/kg, IP, twice per week; hSIRPα-Fc, 1.3 mg/kg, IP, twice per week; HX009, 1.5 mg/kg, IP, twice per week). Tumor volumes and body weights were measured twice per week, and tumor growth inhibition (TGI) was used to determine the anti-tumor activities of each test reagent. The TGI was calculated as $TGI\% = (1\text{-}V_{treatment}/V_{control}) \times 100\%$. The hCD47-MC38 humanized syngeneic model was obtained from Crown Bioscience.

AML-PDX model studies were conducted at Crown Bioscience and essentially followed the same protocol as previously described[28]. Briefly, AM7577, AM5512, and AM8096 leukemic cells were inoculated into NOD-SCID mice via intravenous tail vein injection. Engraftment was confirmed by the presence of circulating human CD45 + cells (anti-human CD45 antibody; Cat. 304038; BioLegend) in the peripheral blood. Mice with successful engraftment of AML-PDXs were randomized into different treatment groups (N = 6) and received their designated treatments. HX009 was intraperitoneally (IP) administrated every two days (Q2D), and cytarabine (Ara-C) was IP administered every day (QD). Following the initiation of designated treatments, leukemic burden was monitored by flow cytometry with anti-human CD45 antibody on the peripheral blood every week, as well as on the peripheral blood, liver cells, bone marrow cells, and splenocytes of mice at sacrifice. Mice were euthanized once the following were observed: body weight loss > 20%, reduced motility and activity, labored breathing, ruffled coat, hunched back, and severe dehydration.

Data availability

Data is provided within the manuscript or supplementary information files.

Received: 2 April 2024; Accepted: 13 November 2024
Published online: 15 November 2024

References

1. Feng, M. et al. Phagocytosis checkpoints as new targets for cancer immunotherapy. *Nat. Rev. Cancer* **19**, 568–586. https://doi.org/10.1038/s41568-019-0183-z (2019).
2. Liu, X., Kwon, H., Li, Z. & Fu, Y. X. Is CD47 an innate immune checkpoint for tumor evasion?. *J. Hematol. Oncol.* **10**, 12. https://doi.org/10.1186/s13045-016-0381-z (2017).
3. Advani, R. et al. CD47 blockade by Hu5F9-G4 and rituximab in non-Hodgkin's lymphoma. *N. Engl. J. Med.* **379**, 1711–1721. https://doi.org/10.1056/NEJMoa1807315 (2018).
4. Folkes, A. S. et al. Targeting CD47 as a cancer therapeutic strategy: the cutaneous T-cell lymphoma experience. *Curr. Opin. Oncol.* **30**, 332–337. https://doi.org/10.1097/CCO.0000000000000468 (2018).
5. Kim, D. et al. Anti-CD47 antibodies promote phagocytosis and inhibit the growth of human myeloma cells. *Leukemia* **26**, 2538–2545. https://doi.org/10.1038/leu.2012.141 (2012).
6. Li, Y. CD47 blockade and rituximab in non-Hodgkin's lymphoma. *N. Engl. J. Med.* **380**, 497. https://doi.org/10.1056/NEJMc1816156 (2019).
7. Yang, K., Xu, J., Liu, Q., Li, J. & Xi, Y. Expression and significance of CD47, PD1 and PDL1 in T-cell acute lymphoblastic lymphoma/leukemia. *Pathol. Res. Pract.* **215**, 265–271. https://doi.org/10.1016/j.prp.2018.10.021 (2019).
8. Liu, X. et al. Dual targeting of innate and adaptive checkpoints on tumor cells limits immune evasion. *Cell Rep.* **24**, 2101–2111. https://doi.org/10.1016/j.celrep.2018.07.062 (2018).
9. Liu, X. et al. CD47 blockade triggers T cell-mediated destruction of immunogenic tumors. *Nat. Med.* **21**, 1209–1215. https://doi.org/10.1038/nm.3931 (2015).
10. Zhou, Z. et al. Tumor-intrinsic SIRPA promotes sensitivity to checkpoint inhibition immunotherapy in melanoma. *Cancer Cell* **40**(1324–1340), e1328. https://doi.org/10.1016/j.ccell.2022.10.012 (2022).
11. Willingham, S. B. et al. The CD47-signal regulatory protein alpha (SIRPa) interaction is a therapeutic target for human solid tumors. *Proc. Natl. Acad. Sci. U. S. A.* **109**, 6662–6667. https://doi.org/10.1073/pnas.1121623109 (2012).
12. Si, Y. et al. Anti-CD47 monoclonal antibody-drug conjugate: A targeted therapy to treat triple-negative breast cancers. *Vaccines* https://doi.org/10.3390/vaccines9080882 (2021).
13. Sikic, B. I. et al. First-in-human, first-in-class phase I trial of the anti-CD47 antibody Hu5F9-G4 in patients with advanced cancers. *J. Clin. Oncol.* **37**, 946–953. https://doi.org/10.1200/JCO.18.02018 (2019).
14. Advani, R., Volkmer, J. P. & Chao, M. P. CD47 blockade and rituximab in non-Hodgkin's lymphoma. *N. Engl. J. Med.* **380**, 497–498. https://doi.org/10.1056/NEJMc1816156 (2019).
15. Chao, M. P. et al. Anti-CD47 antibody synergizes with rituximab to promote phagocytosis and eradicate non-Hodgkin lymphoma. *Cell* **142**, 699–713. https://doi.org/10.1016/j.cell.2010.07.044 (2010).
16. Sharma, P. & Allison, J. P. The future of immune checkpoint therapy. *Science* **348**, 56–61. https://doi.org/10.1126/science.aaa8172 (2015).
17. Ke, H. et al. HX009, a novel BsAb dual targeting PD1 x CD47, demonstrates potent anti-lymphoma activity in preclinical models. *Sci. Rep.* **13**, 5419. https://doi.org/10.1038/s41598-023-32547-y (2023).
18. Liu, R. et al. Phase I study of pucotenlimab (HX008), an anti-PD-1 antibody, for patients with advanced solid tumors. *Ther. Adv. Med. Oncol.* **13**, 17588359211020528. https://doi.org/10.1177/17588359211020528 (2021).
19. Song, Y. et al. HX008, an anti-PD1 antibody, plus irinotecan as second-line treatment for advanced gastric or gastroesophageal junction cancer: a multicenter, single-arm phase II trial. *J. Immunother. Cancer* https://doi.org/10.1136/jitc-2020-001279 (2020).
20. Xu, J. et al. Anti-PD-1 antibody HX008 combined with oxaliplatin plus capecitabine for advanced gastric or esophagogastric junction cancer: a multicenter, single-arm, open-label, phase Ib trial. *Oncoimmunology* **10**, 1864908. https://doi.org/10.1080/2162402X.2020.1864908 (2020).

21. Zhang, J., Huang, Y., Xi, G. & Zhang, F. HX008: a humanized PD-1 blocking antibody with potent antitumor activity and superior pharmacologic properties. *MAbs* **12**, 1724751. https://doi.org/10.1080/19420862.2020.1724751 (2020).
22. Crescioli, S. et al. IgG4 characteristics and functions in cancer immunity. *Curr. Allergy Asthma Rep.* **16**, 7. https://doi.org/10.1007/s11882-015-0580-7 (2016).
23. Buatois, V. et al. Preclinical development of a bispecific antibody that safely and effectively targets CD19 and CD47 for the treatment of B-cell lymphoma and leukemia. *Mol. Cancer Ther.* **17**, 1739–1751. https://doi.org/10.1158/1535-7163.MCT-17-1095 (2018).
24. Cao, X. et al. Targeting macrophages for enhancing CD47 blockade-elicited lymphoma clearance and overcoming tumor-induced suppression. *Blood* https://doi.org/10.1182/blood.2021013901 (2022).
25. Chao, M. P. et al. Therapeutic targeting of the macrophage immune checkpoint CD47 in myeloid malignancies. *Front. Oncol.* **9**, 1380. https://doi.org/10.3389/fonc.2019.01380 (2019).
26. Iwamoto, C. et al. The BALB/c-specific polymorphic SIRPA enhances its affinity for human CD47, inhibiting phagocytosis against human cells to promote xenogeneic engraftment. *Exp. Hematol.* **42**(163–171), e161. https://doi.org/10.1016/j.exphem.2013.11.005 (2014).
27. Yamauchi, T. et al. Polymorphic Sirpa is the genetic determinant for NOD-based mouse lines to achieve efficient human cell engraftment. *Blood* **121**, 1316–1325. https://doi.org/10.1182/blood-2012-06-440354 (2013).
28. An, X. et al. AC220 and AraC cause differential inhibitory dynamics in patient-derived M5-AML with FLT3-ITD and thus, ultimately distinct therapeutic outcomes. *Exp. Hematol.* **45**(36–44), e32. https://doi.org/10.1016/j.exphem.2016.09.004 (2017).
29. Lu, Y. et al. OX40 shapes an inflamed tumor immune microenvironment and predicts response to immunochemotherapy in diffuse large B-cell lymphoma. *Clin. Immunol.* **251**, 109637. https://doi.org/10.1016/j.clim.2023.109637 (2023).
30. Roohullah A et al. First-in-human phase I dose escalation study of HX009, a novel recombinant humanized anti-CD47/PD-1 bispecific antibody, in patients with advanced malignancies. https://ascopubs.org/doi/abs/10.1200/JCO.2021.39.15_suppl.2517 (2021).
31. Yang, H., Xun, Y. & You, H. The landscape overview of CD47-based immunotherapy for hematological malignancies. *Biomark. Res.* **11**, 15. https://doi.org/10.1186/s40364-023-00456-x (2023).
32. Lin, G. H. Y. et al. TTI-621 (SIRPalphaFc), a CD47-blocking cancer immunotherapeutic, triggers phagocytosis of lymphoma cells by multiple polarized macrophage subsets. *PLoS One* **12**, e0187262. https://doi.org/10.1371/journal.pone.0187262 (2017).
33. Piccione, E. C. et al. SIRPalpha-antibody fusion proteins selectively bind and eliminate dual antigen-expressing tumor cells. *Clin. Cancer Res.* **22**, 5109–5119. https://doi.org/10.1158/1078-0432.CCR-15-2503 (2016).
34. Liu, B. et al. Elimination of tumor by CD47/PD-L1 dual-targeting fusion protein that engages innate and adaptive immune responses. *MAbs* **10**, 315–324. https://doi.org/10.1080/19420862.2017.1409319 (2018).
35. Zhang, A. et al. Dual targeting of CTLA-4 and CD47 on Treg cells promotes immunity against solid tumors. *Sci. Transl. Med.* https://doi.org/10.1126/scitranslmed.abg8693 (2021).
36. Piccione, E. C. et al. A bispecific antibody targeting CD47 and CD20 selectively binds and eliminates dual antigen expressing lymphoma cells. *MAbs* **7**, 946–956. https://doi.org/10.1080/19420862.2015.1062192 (2015).
37. Fu, Y., Lin, Q., Zhang, Z. & Zhang, L. Therapeutic strategies for the costimulatory molecule OX40 in T-cell-mediated immunity. *Acta Pharm. Sin. B* **10**, 414–433. https://doi.org/10.1016/j.apsb.2019.08.010 (2020).
38. Ishii, N., Takahashi, T., Soroosh, P. & Sugamura, K. OX40-OX40 ligand interaction in T-cell-mediated immunity and immunopathology. *Adv. Immunol.* **105**, 63–98. https://doi.org/10.1016/S0065-2776(10)05003-0 (2010).
39. Chen, D. X. A. In vivo pharmacology models for cancer target research. In *Target Identification and Validation in Drug Discovery: Methods and Protocols, Methods in Molecular Biology* (eds Moll, J. & Carotta, S.) 183–211 (Springer, 2019).
40. Yang, M. et al. Overcoming erlotinib resistance with tailored treatment regimen in patient-derived xenografts from naive Asian NSCLC patients. *Int. J. Cancer* **132**, E74-84. https://doi.org/10.1002/ijc.27813 (2013).
41. Li, Q. X., Feuer, G., Ouyang, X. & An, X. Experimental animal modeling for immuno-oncology. *Pharmacol. Ther.* **173**, 34–46. https://doi.org/10.1016/j.pharmthera.2017.02.002 (2017).
42. Liu, J. et al. Targeting macrophage checkpoint inhibitor SIRPalpha for anticancer therapy. *JCI Insight* https://doi.org/10.1172/jci.insight.134728 (2020).

Acknowledgements

The authors would like to thank scientists and technicians in West China-Frontier PharmaTech Co., Ltd. (National Chengdu Center for New Drug Safety Evaluation) who performed the cynomolgus monkey experiments, Crown Bioscience, Inc., and Biocytogen, who performed the mouse tumor model studies.

Author contributions

HK, TY, QXL: design the experiments, analyze the data, write manuscript; JPL, XYA, JJW, CC, LXX: design the experiments, analyze the data; FMZ, LZ: oversee the project, discussion of the data, suggest experiments, review/edit manuscript Xianfei He: provide key reagents, discussions and suggestions.

Funding

The study was supported by the R/D budget of the affiliated organizations.

Declarations

Competing interests

The authors are employees of the affiliated organizations listed. The authors declare no competing interests.

Additional information

Supplementary Information The online version contains supplementary material available at https://doi.org/10.1038/s41598-024-79865-3.

Correspondence and requests for materials should be addressed to Q.-X.L.